Available online at www.sciencedirect.com

SciVerse ScienceDirect

Ceramics International 39 (2013) 39–50

CERAMICS INTERNATIONAL

www.elsevier.com/locate/ceramint

Effect of surfactant and heat treatment on morphology, surface area and crystallinity in hydroxyapatite nanocrystals

M. Khalid[a,*], M. Mujahid[a], S. Amin[b], R.S. Rawat[c], A. Nusair[d], G.R. Deen[c]

[a]School of Chemical and Materials Engineering, National University of Sciences and Technology, Sector H-12, Islamabad, Pakistan
[b]PINSTECH, PO Box 1356, Islamabad, Pakistan
[c]NSSE, National Institute of Education, Nanyang Technological University, Singapore
[d]Institute of Industrial Control Systems, Rawalpindi, Pakistan

Received 11 March 2012; received in revised form 29 May 2012; accepted 29 May 2012
Available online 9 June 2012

Abstract

Hydroxyapatite (HA) powders were synthesized by the wet precipitation method, with and without surfactant, under identical processing parameters. These powders were then heat treated at 900 °C for 3 h in air. The detailed characterization of the powders was done by using SEM, dynamic light scattering, nitrogen adsorption, XRD, Raman spectroscopy, and FTIR techniques. The HA phase, identified by well defined PO_4^{3-} and OH^- ion peaks in Raman and FTIR spectra, was observed in all the powder samples. The addition of surfactant changed the morphology of the particles from spherical to needle/rod-like structure and increased the surface area up to three times (from 33 to 96 m^2/g). Also, suppression in the evolution of β-TCP phase was observed along with decrease in the crystal size and crystallinity of the powder due to the addition of surfactant. Synthesized nano-HA crystals were found to have diameters and lengths in the range 10–25 nm and 75–150 nm, respectively. The heat treatment changed the architecture of the particles, increased the crystallinity and reduced the surface area to $\approx 7\ m^2/g$. However, the relative increase in crystallinity was much higher for the powder synthesized with surfactant. The ratio of the average crystallite size to the crystallinity degree was about 0.53 ± 0.07 for all the powders. The particle size distribution was bimodal and coarser for the powder synthesized without surfactant. The pore size analysis showed transformation of a predominantly mesoporous structure into a meso- plus macroporous one on heat treatment. The intensity of OH^- group peak in Raman spectra was found to be highly sensitive to the crystalline state of the HA powder and may be used to assess crystallinity.

Keywords: Hydroxyapatite; Surfactant; Surface area; Crystallinity

1. Introduction

Apatites are the most important constituents of hard human tissues like bones and teeth. Therefore intensive research is going on these materials for the last several decades. Amongst the apatites, hydroxyapatite (HA) is the most important one as its chemical composition is similar to the inorganic part of human bones and teeth. It is one of the few materials which have the characteristics of biocompatibility, bioactivity and osteoconductivity. It has a wide range of applications like treatment of bone defects, coatings for dental and orthopedic implants, craino-maxillofacial reconstruction and spinal surgery [1,2]. It is also used in variety of applications like lighting materials, catalyst support, chromatographic columns, chemical sensors, ion conductors, agents for drug delivery and preventing proliferation of cancer cells [3–6]. For each of the applications there are specific requirements in terms of morphology, particle size, particle size distribution, crystallinity and purity level. For example, their use as coatings on medical implants demands high crystallinity for enhanced stability in physiological conditions [7]. However, for the removal of heavy ions like Pb^{2+} and Zn^{2+} from waste water, low crystallinity and high specific surface area of HA powders are desirable [8]. It has also been shown

*Corresponding author. Tel.: +92 333 561 4466.
E-mail address: semelkhalid@hotmail.com (M. Khalid).

0272-8842/$36.00
http://dx.doi.org/10.1016/j.ceramint.2012.05.090

that protein adsorption on HA particles is influenced by the volume of micropores in the examined samples; and powders with higher amount of micropores adsorb more protein [9]. The phase composition of calcium phosphates (HA, α-TCP, β-TCP etc.) is another important characteristic that defines the dissolution, and hence the bioactivity, of a particular phase [10]. Moreover, it is well known that nano-grained ceramics could be sintered at comparatively low temperatures as compared to micro-grained counterparts.

A number of routes have been used for the synthesis of hydroxyapatite (HA) that include the sol–gel method [11,12], solid-state reaction method [13,14], hydrothermal method [15,16], template-directed method [17,18] and micro-emulsion method [19,20]. However, amongst them all, the wet chemical precipitation method is an easy way to prepare HA powders. The type of processing route adopted and the synthesis conditions used affect the morphology, particle size distribution, the degree of crystallinity, phase purity, specific surface area and the porosity of the HA powders, which ultimately define its use for a particular application.

The chemically synthesized HA particles may have different morphologies like spheres, needles, rods, fibers, plates etc. However, the needle or rod-like morphology of HA is preferred and is of great interest for the researchers. This is due to the fact that HA like crystals are arranged in those morphologies in human calcified tissues having dimensions of $25 \times 4 \times 2\ nm$ and $35 \times 25 \times 4\ nm$ for bone and dentin, respectively, as given in review [21] and references therein. Therefore, to mimic the properties of natural bone, researchers would like to synthesize HA crystals with the morphology and the size mentioned above. To control the morphology and to reduce the particle size different surfactants/dispersants like cetyltrimethyl ammonium bromide (CTAB), polyethylene glycol (PEG), sodium dodecyl sulfate (SDS), citric acid, ethanol amine and polyvinyl alcohol (PVA) have been utilized [6,17,18,22–29]. CTAB is a biocompatible cationic surfactant which ionizes in aqueous solutions to generate positively charged monomers. These monomers then self-assemble and act as nucleating sites to adsorb $(PO_4)^{3-}$ first and then Ca^{2+} ions on their surfaces to produce HA crystals through precipitation phenomena [30].

The synthesis conditions like temperature, pH and CTAB concentration strongly affect the morphology, size and phases of HA and other calcium phosphate particles [5,6,23,29,30]. Li et al. synthesized HA particles using CTAB:PO_4^{3-} = 1:1 proportion at 40, 80, 120 and 160 °C, and reported the elongation of HA rods at higher temperatures [23]. They employed $CaCl_2$ and $K_2HPO_4 \cdot 3H_2O$ as Ca and P sources, respectively. It is also reported that efficacy of CTAB to alter HA morphology was more prominent when solution pH was maintained at 9 as compared to solution pH of 13 under hydrothermal conditions using $CaCl_2$ and H_3PO_4 precursors [5]. HA nanostructures with diameters/widths and lengths of 27–120 nm and 200–1000 nm, respectively, were obtained when CTAB concentration employed was in the range 170–240 mM [5,29,30]. However, the change in morphology was not evident when comparatively smaller concentration of CTAB (5–30 mM) was used in hydrothermal environment [26]. In that study [26], only spherical/slightly elongated particles were observed, although the concentration selected was above the critical micelle concentration (CMC) of 0.9–1.0 mM. The use of CTAB in aqueous solutions above CMC promotes rod-like micelles [31] and consequently HA needles/rods were expected. In the present study, HA powders were synthesized using the wet precipitation method with and without a surfactant. The purpose is to evaluate and compare the effect of surfactant addition and heat treatment on morphology, size, crystallinity, surface area and porosity of chemically precipitated HA crystals.

2. Experimental methods and procedures

2.1. Synthesis of powders

HA powders were synthesized by two routes: (i) without any surfactant—hereafter referred to as 'NoSurf', and (ii) with surfactant—hereafter referred to as 'Surf'. In the first ('NoSurf') route, the HA particles were synthesized with calcium nitrate tetrahydrate ($Ca(NO_3)_2 \cdot 4H_2O$) as a calcium source, diammonium hydrogen phosphate ($(NH_4)_2HPO_4$) as a phosphorous source and ammonia solution as an agent for pH adjustment. In the synthesis process, first a solution was prepared by dissolving 262.5 g of $Ca(NO_3)_2 \cdot 4H_2O$ in 1600 ml of distilled water by heating it at 80 °C with continuous stirring. Similarly, a second solution was prepared with 76 g of $(NH_4)_2HPO_4$ dissolved in 1100 ml of distilled water under the same conditions. The pH of $(NH_4)_2HPO_4$ solution was adjusted to 12 by adding ammonia solution before the drop-wise addition of $Ca(NO_3)_2 \cdot 4H_2O$ solution into it. It is reported that the pH greater than 10 is beneficial for obtaining pure HA [6]. The whole mixture was then stirred and heated at 80 °C for 2 h. The solution was then left for 24 h for precipitation of HA crystals, followed by washing in distilled water. The precipitated powder was dried and calcined at 80 °C for 24 h and at 550 °C for 2 h in air, respectively.

The chemical reaction for the synthesis of HA can be described by the following equation:

$$10Ca(NO_3)_2 \cdot 4H_2O + 6(NH_4)_2HPO_4 + 8NH_4OH \rightarrow Ca_{10}(PO_4)_6(OH)_2 + 20NH_4NO_3 + 46H_2O$$

In the second route ('Surf'), cetyltrimethyl ammonium bromide (CTAB) was used as surfactant to prepare HA crystals by employing the same synthesis conditions as used in the first route ('NoSurf'). The only difference was the addition of the CTAB solution (36.5 g of CTAB dissolved in 500 ml of distilled water) to the $(NH_4)_2HPO_4$ solution before the $Ca(NO_3)_2 \cdot 4H_2O$ solution was transferred to it drop-wise. Synthesis conditions such as precursors for Ca and P, pH, temperature and reflux time were kept constant for the both routes under ambient

pressure. The CTAB concentration was 60 mM that falls between the concentrations used in some previous investigations [5,26,29,30] and was expected to produce nanorods/needles of HA with dimensions similar to the ones found in natural bone and dentin. Moreover, shorter reflux time (2 h instead of the more common 24 h) was employed, making the process economical. After synthesis, the powders produced by two routes ('Surf' and 'NoSurf') were heat treated at 900 °C for 3 h in air at a heating rate of 15 °C/min followed by cooling in the furnace. The powders 'Surf' and 'NoSurf' are designated as 'Surf-900C' and 'NoSurf-900C', respectively, after the heat treatment. The synthesis conditions and heat treatment employed are summarized in Table 1. The concentrations of CTAB mentioned were calculated by the amount of CTAB dissolved in combined volume of water used to dissolve both CTAB and PO_4 precursor.

2.2. Characterization of powders

2.2.1. Morphological analysis by SEM

Surface morphology of all the powders ('Surf', 'Surf-900C', 'NoSurf' and 'NoSurf-900C') was analyzed by a scanning electron microscope (SEM), Jeol JSM-6490A. A field emission scanning electron microscope (FESEM), Jeol JSM-6700F, was also used for the analysis of powders 'Surf' and 'NoSurf'. The samples for SEM were prepared by placing the powders on the conductive carbon tape without any ultrasonic dispersion. For FESEM analysis, the powders were dispersed ultrasonically in ethanol for 30 min. A drop of this dispersed solution was then placed on silicon wafer and was dried. Finally, the samples were gold coated by sputtering to avoid charging.

2.2.2. Particle size distribution

The particle size distribution was determined by the dynamic light scattering (DLS) technique using a Malvern Zetasizer ZS90 with laser of wavelength 632 nm. For DLS measurements, the HA powder was dispersed in dilute deionised water by ultrasonication for 30 min at room temperature before transferring it to the measurement cell. The analysis was carried out 3 times and averaged.

2.2.3. Surface area and porosity analysis

Surface area and porosity of the powders were investigated by adsorption of N_2 at 77 K using a gas adsorption analyzer Micromeritics ASAP 2020. Prior to N_2 adsorption, the powders were degassed for 3 h at a temperature of 350 °C and a pressure of 5 mm Hg. The surface area of the powder was determined according to the Barrett–Emmett–Teller (BET) equation, while the pore volume and pore width were calculated from the adsorption data of isotherms in accordance to the Barrett–Joyner–Halanda (BJH) model.

2.2.4. Phase analysis by XRD

Phase analysis was carried out on a Siemens D5005 X-Ray diffractometer in locked couple mode using CuKα radiation with the scan step size of 0.02° and 3 s dwell time per step. The diffractometer was operated at 40 kV and 40 mA.

2.2.5. Raman spectroscopy

Raman spectroscopy was performed for verifying functional groups such as $(PO_4)^{3-}$ and $(OH)^-$ using a Renishaw inVia Raman microscope. The wavelength of the laser used was 532 nm. The samples were scanned in the range 1200–200 cm^{-1} and 3500–3640 cm^{-1} with spectral resolution of 1 cm^{-1}.

2.2.6. FTIR analysis

The presence of functional groups was also investigated by the Fourier transform infrared (FTIR) spectroscopy. A mixture of synthesized powder and spectroscopic grade KBr was ground in an agate mortar and was pressed at 10,000 Psi in a stainless steel die to obtain thin transparent pellet. FTIR spectra were collected by a Perkin-Elmer Spectrum 100 FTIR spectrometer in the spectral range 4000–400 cm^{-1} with a resolution of 4 cm^{-1}.

3. Results and discussion

3.1. SEM analysis

The SEM images of powders 'NoSurf', 'Surf', 'NoSurf-900C', and 'Surf-900C' are shown in Fig. 1(a)–(d). Fig. 1(a) and (c) shows that before the heat treatment the HA particles are mostly agglomerated nano particles, with the particles of powder 'Surf' being finer and more porous than powder 'NoSurf'. After the heat treatment, the nano particles coalesce for both types of powders and an interconnected porous structure of micron sized

Table 1
Synthesis conditions and heat treatment employed for HA powders.

Nomenclature	Synthesis conditions				Heat treatment
	Surfactant	Refluxing	Drying	Calcination	
NoSurf	No	80 °C, 2 h	80 °C, 24 h	550 °C, 2 h	No
NoSurf-900C	No				900 °C, 3 h
Surf	CTAB				No
Surf-900C	CTAB				900 °C, 3 h

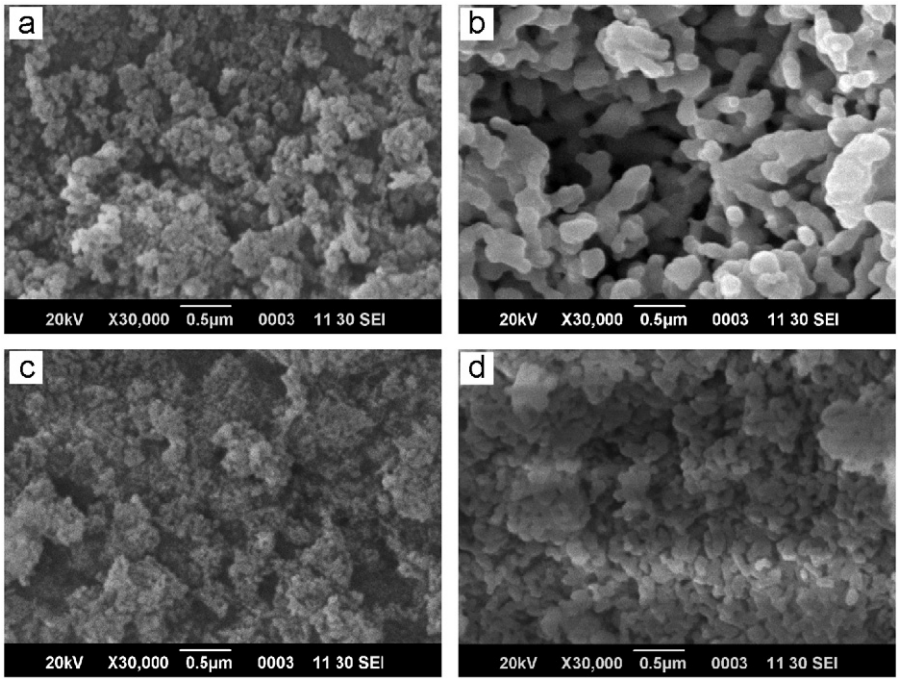

Fig. 1. SEM micrograph exhibiting morphology and microstructure of the particles before and after the heat treatment: (a) powder 'NoSurf', (b) powder 'NoSurf-900C', (c) powder 'Surf' and (d) powder 'Surf-900C'.

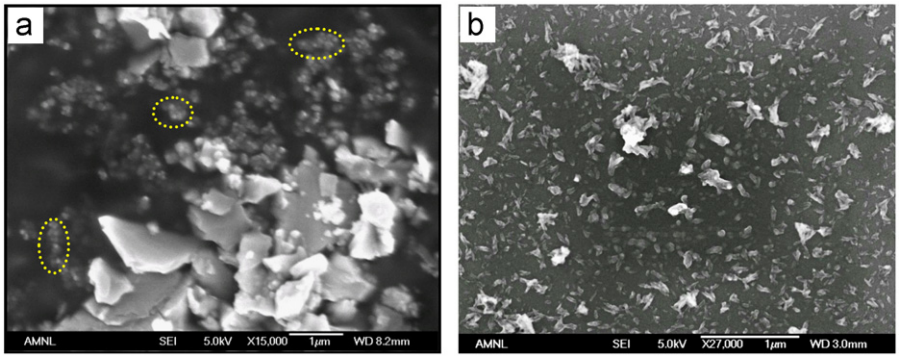

Fig. 2. FESEM images exhibiting morphology of the particles: (a) Powder 'NoSurf', showing the presence of spherical particles, agglomerates (encircled) and large particles and (b) powder 'Surf', showing rod/needle-like morphology of the particles.

particles is evolved, as shown in Fig. 1(b) and (d). Once again the features of powder 'Surf-900C' are finer as compared to those of powder 'NoSurf-900C'. Necking among the coalesced particles is clearly seen in heat treated powders which is an indication that sintering has started at 900 °C. The above mentioned features were observed when the SEM analysis was carried out without dispersing the powders by ultrasonic treatment. Powders 'Surf' and 'NoSurf' were also analyzed by FESEM after ultrasonic dispersion in ethanol, and the results are shown in Fig. 2.

The morphology of HA particles is influenced by many factors such as pH, temperature, concentration of precursors, and dispersant species during the synthesis process [6,24,25,29,32]. Sphere like HA particles are reported at pH = 11, 150 °C, and plate morphology at pH = 6, 150 °C [32]. In the current investigation (pH = 12, 80 °C), the morphology of the particles of powder 'NoSurf' is spherical as well as plate-like. The plate-like particles are much larger in size. Some particles in the form of agglomerates (encircled in Fig. 2a) are also seen. The spherical particles are about 40–60 nm in diameter, while the large particles/plates are between 200 nm and 1.5 µm in length. Similar spherical particles (50–100 nm) of HA are reported when no surfactant was used under hydrothermal conditions [29]. In the current study, the presence of sphere and thick plate-like morphology in powder 'NoSurf' could be explained on the assumption that first a random precipitation of HA crystals in the form of spheres predominated and then the growth of some spherical particles occurred preferably in one direction that resulted in the evolution of

thick plate-like morphology. Plate-like morphology has also been reported [32] but under different synthesis conditions as mentioned above.

On the other hand, the morphology of the particles of powder 'Surf' is predominantly rod/needle type as shown in Fig. 2b, although some spherical particles are also observed. Rods are about 10–25 nm in diameter and 75–150 nm in length. In a previous study, the rods with the diameter of about 50–120 nm and about 200–700 nm long with the use of CTAB (170 mM), are also reported in hydrothermal environment [29]. In another investigation, the needles of about 27 nm in diameter and 255 nm in length are reported by using CTAB (240 mM) under hydrothermal conditions [5]. Yao et al. have shown the formation of 50–100 nm thick and 500–1000 nm long HA nanostructures by employing CTAB (240 mM) using the wet precipitation route [30]. Rod-like morphology in the current and previous reports could be linked to the fact that the concentration of CTAB used was above its critical micelle concentration (CMC) of 0.9–1.0 mM. The use of CTAB in aqueous solutions above CMC promotes rod-like micelles [29,31] and HA crystals may then precipitate on these micelles in the form of rods. In the present study, 60 mM of CTAB was used which is well above the CMC and subsequently promoted rod-like growth. The formation of finer HA nanorods in the current study could be attributed to the smaller concentration of the CTAB employed as compared to previous reports [5,29,30]. The important features of utilizing comparatively less CTAB concentration in the present study is that the needles/rods (10–25 *nm* in diameter and 75–150 *nm* in length) produced are closer to natural HA crystals ($25 \times 4 \times 2$ nm and $35 \times 25 \times 4$ nm) found in bone and dentin [21] as well as making the synthesis process economical. Aside from CTAB, rod-like morphology of HA particles is also reported by employing citric acid as a surfactant [33].

It is also observed that the particles size distribution for powder 'Surf' (Fig. 2b) is more uniform as compared to powder 'NoSurf' (Fig. 2a). The reason for this uniform distribution of particles by using surfactant may be explained by the fact that the surfactant provided more nucleation sites for the precipitation of HA, resulting in inhibited growth of precipitated particles/needles randomly.

3.2. Particle size distribution

Particle size measurement was carried out by the dynamic light scattering (DLS) technique and the results for powders produced without surfactant ('NoSurf') and with surfactant ('Surf') are shown in Fig. 3(a) and (b). Fig. 3b shows that the particle size distribution is bimodal (having two distributions) for powder 'NoSurf'. The range of particles is 140–400 nm for the first distribution and 700–2000 nm for the second one. This bimodal distribution of HA particles is also evident from the SEM image (Fig. 2a) where smaller spherical particles and larger particles in the form of plates are clearly observed. It is also observed that the particles (140–400 nm) of the first distribution measured by the DLS technique (Fig. 3b) are larger compared to the particles (40–60 nm) revealed by FESEM analysis (Fig. 2a). This difference could be attributed to the agglomeration of the small particles into clusters, which are measured by DLS. These clusters of particles are also visible in FESEM analysis (encircled agglomerates in Fig. 2a). In the case of second distribution (relating to large particles in the form of thick plates), the particle size measured by DLS (Fig. 3b) is consistent with the size revealed by FESEM image (Fig. 2a) but the fraction of large particles (in the form of thick plates) seems to be smaller in DLS measurement (Fig. 3b, 2nd distribution) as compared to FESEM analysis (Fig. 2a). A possible reason for this difference is that some large particles may have settled down during DLS measurement.

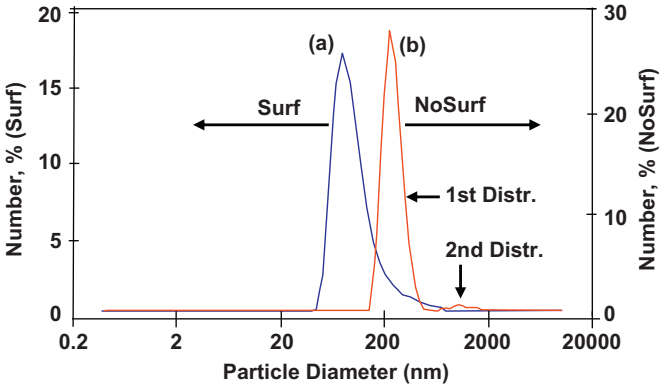

Fig. 3. Particle size distribution of powders by dynamic light scattering technique: (a) powder 'Surf' and (b) powder 'NoSurf'.

On the other hand, the particle size distribution for powder 'Surf' is unimodal (Fig. 3b) and the size range is 40–400 nm which is centered at 80 nm diameter. These features are consistent with FESEM observation (Fig. 2b). The particles that are above 150 nm in DLS measurement (Fig. 3b) could again be linked to the particles agglomeration.

Comparing the particle morphology and size distribution (by SEM and DLS) of powders synthesized by two routes, it can be deduced that CTAB has changed the morphology of HA particles from sphere to rod-like. Secondly, it also acts as a nucleating site and helps to produce HA particles with more uniform and finer size distribution.

3.3. Surface area and porosity analysis

N_2 adsorption isotherms of synthesized HA powders are shown in Fig. 4a–d. It is observed that much larger amount (about 400 cm^3/g) of N_2 is adsorbed on powder 'Surf' than that of powder 'NoSurf' (about 82 cm^3/g). It is also revealed that before the heat treatment (powder 'Surf' and 'NoSurf') adsorption starts at very low P/P^o value and there is a gradual increase in the adsorbed quantity prior to the onset of an abrupt increase in adsorption due to

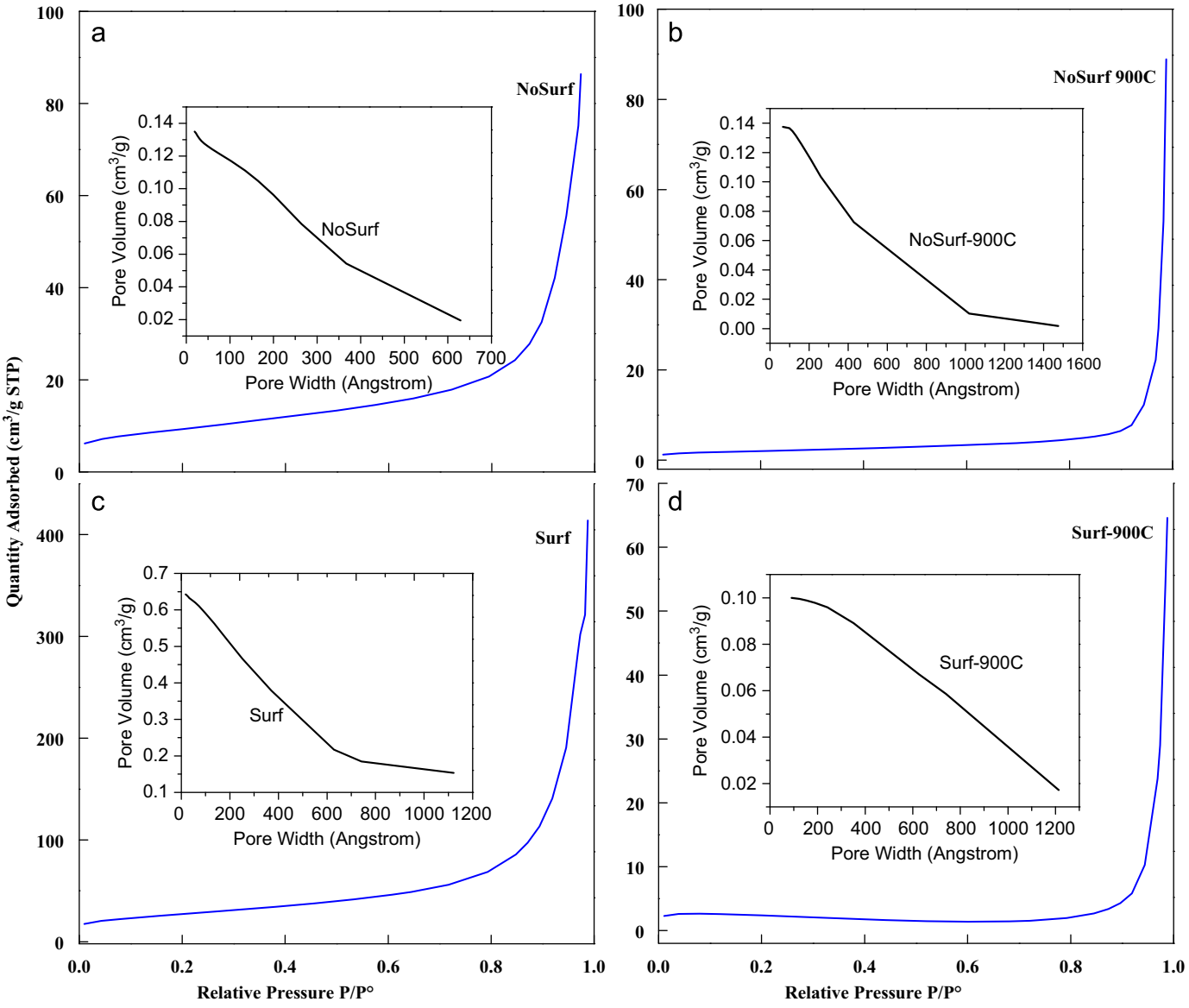

Fig. 4. Adsorption isotherms for powders: (a) 'NoSurf', (b) 'NoSurf-900C', (c) 'Surf', and (d) 'Surf-900C'. Pore widths distributions are shown in insets.

capillary condensation at $P/P^{o} \approx 0.9$. Whereas, after the heat treatment (powder 'Surf-900C' and 'NoSurf-900C'), there is a little adsorption before $P/P^{o} \approx 0.9$. It means that adsorption is easier on non-heat treated powders at low pressures.

Pore size distributions (shown in insets in Fig. 4) are 2–63 nm, 6–100 nm, 2–70 nm and 9–120 nm for the powders 'NoSurf', 'NoSurf-900C', 'Surf' and 'Surf-900C', respectively. Analysis of this data indicates two trends. Firstly, the fine pores (< 5 nm) have collapsed, and secondly, the pore size distribution has widened towards higher pore widths after the heat treatment. It means that the shrinkage in HA particles has occurred and a predominantly mesoporous HA structure has changed to meso- plus macroporous one upon heating at 900 °C.

BET surface area, cumulative pore volume and average pore width derived from N_2 adsorption isotherms are shown in Fig. 5a–c. It is observed that powder 'Surf' has higher surface area (96 m^2/g) than that of powder 'NoSurf' (area = 33 m^2/g). It may be explained on the basis that the surfactant (CTAB) evaporated during the synthesis process of powder 'Surf' (calcination at 550 °C), inducing very fine pores. This hypothesis is corroborated by the studies in which evaporation of CTAB from HA powders has been reported in the temperature range 200–550 °C by thermogravimetric analysis [23] and the formation of nano sized pores along the length of HA rods as evidenced by TEM analysis when the HA powder, synthesized with CTAB (240 mM), was calcined at 550 °C [30]. The pores among the agglomerated particles (Fig. 1c) may also contribute to the overall surface area of this powder ('Surf'). Moreover, the surfactant also acted as a template/nucleating site and inhibited the particle growth that might result in higher surface area. Similar surface area (of about 88 m^2/g) for

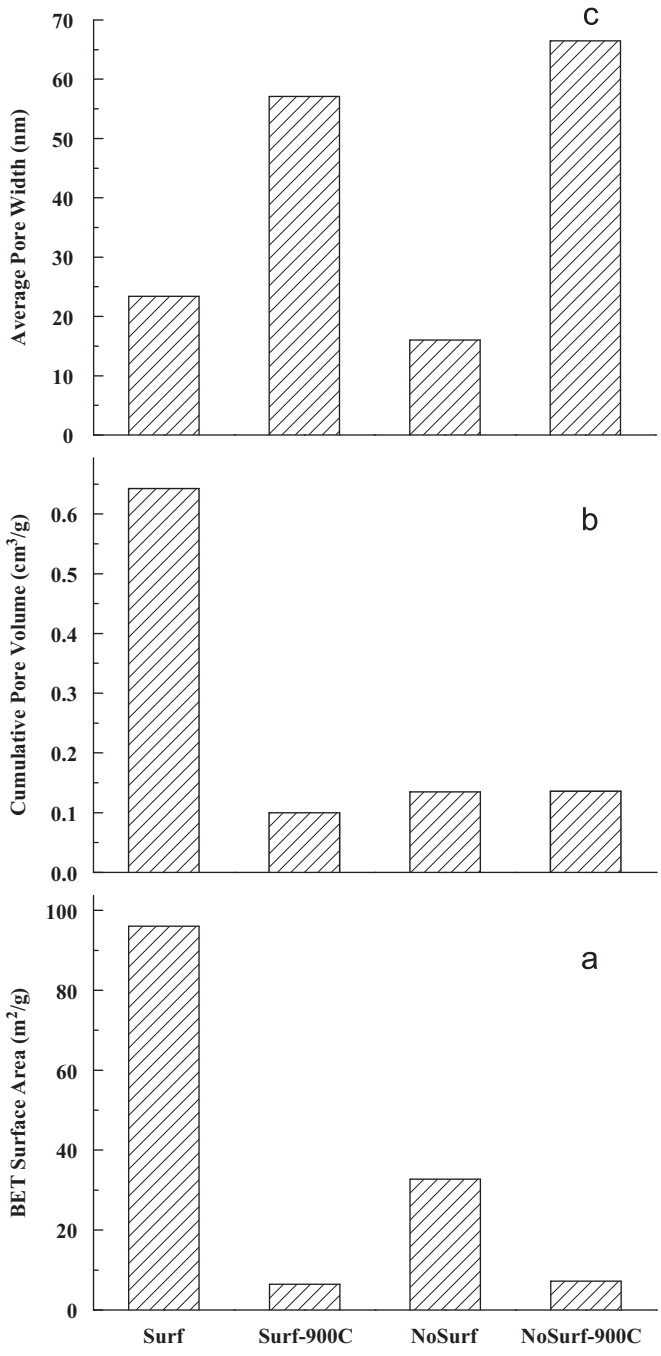

Fig. 5. Characteristics of powders derived from adsorption isotherms for synthesized powders: (a) BET surface area (b) cumulative pore volume and (c) average pore width.

HA powder is reported by the use of CTAB [29]. However, much higher surface area ($>200\ m^2/g$) was obtained for mesoporous calcium phosphate using non-ionic surfactant in un-calcined condition [27] at synthesis temperature of 25 °C. In that work [27], the surface area reduced to about $90\ m^2/g$ when the synthesis temperature was raised to 80 °C. In the current study, the surface area of about $96\ m^2/g$ obtained at process temperature of 80 °C (powder 'Surf') is comparable to the surface area obtained in the work [27] at process temperature of 80 °C using a non-ionic surfactant. It shows that the process temperature is an important parameter in controlling the surface area of HA crystals irrespective of the kind of surfactant used.

In case of the powder synthesized without surfactant ('NoSurf'), it is assumed that the pores were created only among the agglomerated particles (Fig. 1a) and fine pores induced by the evaporation of surfactant were absent. Consequently, there were comparatively less number of fine pores in this powder that resulted in lower surface area ($33\ m^2/g$). This hypothesis is also supported by the presence of higher proportion of fine pore volume for powder 'Surf' as compared to powder 'NoSurf' which is indicated by insets in Fig. 4a and c. The other possible reason for lower area is the presence of large particles, evidenced by both FESEM imaging (Fig. 2a) and DLS measurement (Fig. 3b), in this powder ('NoSurf').

The heat treatment of powder 'Surf' at 900 °C reduced the surface area from 96 to $6\ m^2/g$. A similar trend of reduction in surface area ($32–7\ m^2/g$) upon heating is observed for powder 'NoSurf', but the relative reduction is much smaller as compared to powder 'Surf'. In fact, the two powders have reduced to more or less similar surface area after heat treatment at 900 °C for 3 h. This reduction in surface area could be associated to the assumption that the fine pores on the surface of the particles and among the agglomerated ones would have collapsed by heat treatment at 900 °C. And the particles/grains/crystals coalesced together and shrank, resulting in the formation of larger pores. This assumption is supported by the SEM analysis (Fig. 1) where the agglomerated particle structure before the heat treatment [Fig. 1 (a&c)] was transformed to an interconnected semi-sintered structure by coalescence of particles after the heat treatment [Fig. 1 b and d]. The absence of fine pores having size less than 5 nm (insets of Fig. 4) and enhancement in the average pore width (Fig. 5c) in heat treated powders also validate this assumption. Melville et al. [34] reported that the heat treatment of HA crystals at 900 °C for 1 h resulted in an area equal to $8\ m^2/g$ which is close to the one ($6–7\ m^2/g$) observed in the present study after the heat treatment. Analysis of Melville et al. work [34] and present investigation suggests that heating the chemically precipitated HA crystals at 900 °C results in a similar area irrespective of initial surface area and treatment time.

It is also observed that the cumulative pore volume (Fig. 5b) is the highest for powder 'Surf' in accordance to the highest surface area for this powder (Fig. 5a). Again, the decrease in pore volume (from 0.64 to $0.1\ cm^3/g$) after heating powder 'Surf' is observed but it remains constant ($\approx 0.13\ cm^3/g$) for powder 'NoSurf' before and after heating (Fig. 5b).

Overall, the careful analysis of adsorption isotherms implies that the powders have more surface area, more pore volume and are predominantly mesoporous before the heat treatment. Hence, these powders ('Surf' and 'NoSurf') may be better suited for applications that require adsorption of species like proteins and cells on their

surfaces for biomedical applications and may prove more bioactive as compared to the heat treated ones ('Surf-900C' and 'NoSurf-900C'). Among non-heat treated powders, the powder prepared with surfactant ('Surf') could be more effective. The above mentioned proposition may also be true for removal of heavy ions like Pb^{2+} and Zn^{2+} from waste water in addition to biomedical applications [8,9].

3.4. XRD of the powders

XRD patterns of the powders are shown in Fig. 6. All the powders show predominantly a HA phase except one small β-TCP peak observed in powder 'NoSurf-900C'. A shoulder of β-TCP is also observed in the pattern of powder 'NoSurf' that developed into a well resolved small peak upon heating at 900 °C (powder 'NoSurf-900C'). No β-TCP phase is detected in powder 'Surf-900C'. The standard diffraction data cards used for HA and β-TCP phase identification were JCPDS 09-0432 and 09-0169, respectively. Appearance of β-TCP phase in the powder prepared without surfactant could be explained as follows.

Synthesis of HA phase in calcium phosphates is dependent on the reaction parameters, especially pH, temperature and stirring rate. One recent study showed that pH greater than 10 was beneficial to obtain pure HA phase [6]. In that study, the researchers synthesized HA powders at initial pH of 8, 9, 10 and 11 at process temperature of 40 °C using the chemical precipitation method. In their XRD patterns a high intensity β-TCP peak appeared at pH = 8, whose intensity decreased greatly at pH = 9 (both HA and β-TCP peaks appeared) and it completely disappeared at pH = 10 and pH = 11. The authors correlated the appearance of β-TCP with change in morphology of the precipitated phase with corresponding change in pH. A predominant β-TCP phase (with minor HA phase) has also been reported in another work at pH = 8 [35]. In contrast to these two above mentioned reports, pure HA phase has also been observed at pH = 6, 7 and 9.2 [32]; at pH = 6, 9 and 14 [16]; and at pH = 6.5–7.5 [36] under different processing conditions. It means that achieving a pure HA phase in the wet precipitation method is a complicated process which may depend on the combined effect of synthesis conditions like pH, temperature and reflux time etc. In this regard only a set of precise synthesis conditions may produce a pure HA phase. The CTAB is a cationic surfactant and ionizes in aqueous solutions completely, creating cations (CTA^+) possessing tetrahedral structure. Similarly $(PO_4)^{3-}$ ion is also tetrahedral. Due to charge and stereochemistry complementarity, $(PO_4)^{3-}$ ions could be bound to existing nuclei/micelles (CTA^+). The addition of Ca^{2+} into the solution results in the formation of $Ca_9(PO_4)_6$ clusters having tetrahedral structure which are favorably adopted by the identical hexagonal arrangement of micellar rods of CTAB. Further, optimized reaction conditions favor more Ca^{2+} and OH^- on $Ca_9(PO_4)_6$ clusters through reflux. Subsequently, the growth of HA particles takes place on these micelles as explained in previous reports [5,17,29,30]. It means that CTAB acts as a regulating agent in crystallization and growth of HA particles. In the present study when HA is synthesized without any surfactant/template, there are possibilities that some particles grow into bigger ones and phases other than HA may develop. One of the plausible reason is that inside the bigger particles the reaction conditions, required for HA phase, may not be reachable to some extent from the bulk reaction mixture. On the other hand, in synthesis with surfactant, each CTAB micelle would have acted as a separate reactor and did not allow the particles to grow or agglomerate, and hence, the conditions of the reaction mixture (necessary to form pure HA) were distributed uniformly all over. As a result, pure HA (without β-TCP) was formed using CTAB. The presence of the bigger particles in powder 'NoSurf' is evidenced by the FESEM image (Fig. 2a) and DLS measurement (Fig. 3b). Since, in the present study, there was no difference in synthesis conditions between the two routes except the use of CTAB, and a minor β-TCP phase appeared only in the powder synthesized

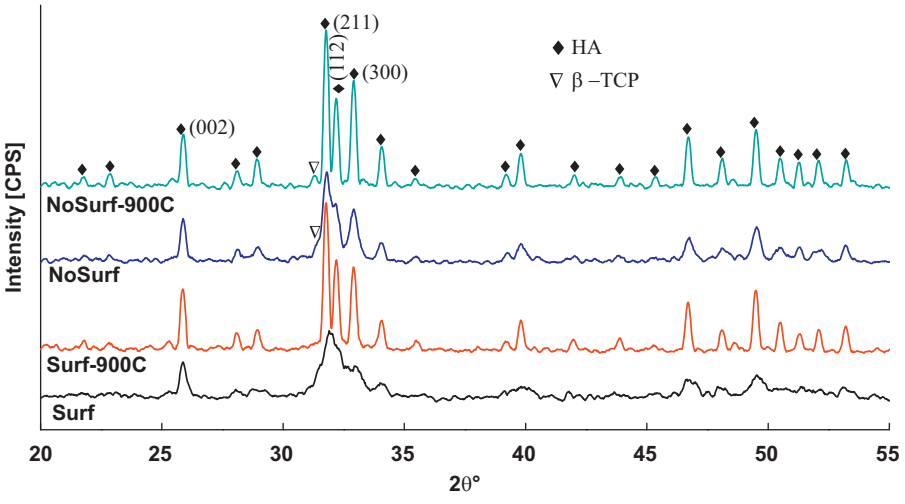

Fig. 6. XRD patterns of synthesized powders. From bottom to top: powder 'Surf', 'Surf-900C', 'NoSurf' and 'NoSurf-900C'.

without CTAB, it may be inferred that CTAB played a role in suppressing β-TCP phase formation under the given conditions.

Summarizing, it could be inferred that the use of CTAB not only affected the particle size and morphology of HA but also helped to produce a pure HA phase (without β-TCP) at controlled reaction parameters.

3.4.1. Determination of average crystallite size and crystallinity degree

The average crystallite size of the powders is inversely proportional to the peak width according to the Scherrer equation [37]:

$$\Delta(2\theta) = \frac{0.9\lambda}{DCos(\theta)}$$

where $\Delta(2\theta)$ represents the peak width at half of the maximum intensity of the (002) reflection, λ is the wavelength for CuKα (0.154056 nm), D is the average crystallite size in nanometers and θ is the Bragg angle.

The crystallinity degree (Xc) of powders was calculated using the relation [36]

$$Xc \approx 1\text{-}(V_{112/300}/\ I_{300})$$

where $V_{112/300}$ is the intensity of the hollow between (112) and (300) reflections that disappears completely in non-crystalline samples, while I_{300} is the intensity of (300) reflection.

The average crystallite size and the crystallinity degree of synthesized powders are shown in Fig. 7. The HA powder synthesized using surfactant ('Surf') exhibits the lowest average crystallite size of about 6 nm. On the other hand, HA synthesized without using surfactant ('NoSurf') shows the average crystallite size of about 30 nm. This could be explained on the basis that since powder 'Surf' has more surface area (Fig. 5a), and hence, it would have more disordered atoms on the surface, resulting in higher peak broadening. Secondly, the synthesis conditions prevailing in the process using surfactant may result in smaller crystallite size inherently. It is also observed that the average crystallite size increases for both powders when they are heat treated at 900 °C. The trend of increasing the crystallite size by heating is also depicted in XRD patterns (Fig. 6) by enhancement in peak intensities for both types of powders. The analysis of data shows that crystallite size of HA crystals can be increased by heat treatment and by preparing them without surfactant. Similar trends in crystallinity degree (%) are observed for all the powders. The increase in crystallinity degree of HA powder with heating was also observed previously [25].

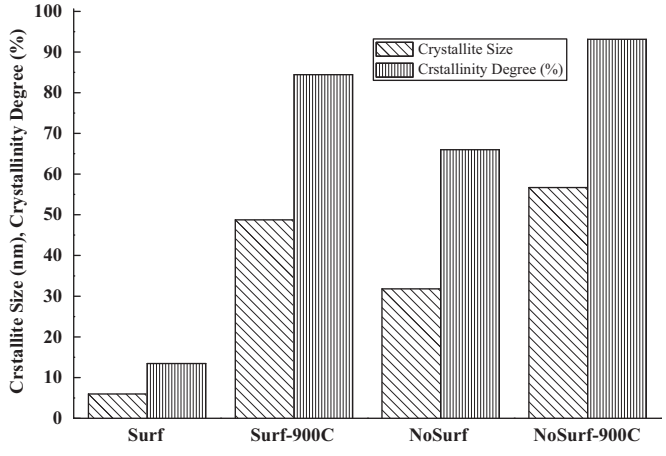

Fig. 7. Crystallite size and crystallinity degree of synthesized powders.

One interesting observation is that the ratio of the average crystallite size (nm) to the crystallinity degree (%) is 0.53 ± 0.07 for both types of powders before and after the heat treatment. It shows a direct relationship between them despite the fact that the two parameters have been measured by different methods.

It is reported that the dissolution rate of hydroxyapatite in vivo depends on the composition and the crystallinity of the powder produced such that the higher the crystallinity, the lower the dissolution rate [38]. The applications such as coating of HA on metallic implants require higher crystallinity to make the coating stable in vivo, while other applications such as scaffolds for bone repair demand controlled dissolution of HA in vivo. It is observed in the current study that heat treatment can be applied to change the crystallinity of HA crystals, and hence, it may be utilized accordingly. Another noteworthy point is that the decomposition of HA phase was not observed by heating, up to 900 °C, for both types of powders.

3.5. Raman spectroscopy

To evaluate the presence and the state of functional groups associated with HA, Raman spectra of the powders were collected and are shown in Fig. 8a and b in two scan ranges. Depending on the crystallinity and the phase, vibration modes due to $(PO_4)^{3-}$ tetrahedra normally appear in hydroxyapatite and other calcium phosphates at four different frequency ranges [39]. It consists of the ν_1 symmetric stretching mode (P–O bonds), ν_3 asymmetric stretching mode (P–O bonds), ν_2 bending mode (O–P–O bonds) and ν_4 bending mode (O–P–O bonds). The peaks appearing in the current study are designated as follows.

Peaks in the range 400–480 cm^{-1} can be assigned to the ν_2 mode, 575–615 cm^{-1} range to the ν_4 mode, intense peak at 962.75 cm^{-1} to ν_1 mode and in range of 1025–1080 cm^{-1} to the ν_4 mode, which are in accordance to the work reported in reference [40]. Small peaks appearing in Raman spectra in the range 200–350 cm^{-1} could be due to the translational modes of Ca^{2+} and PO_4^{3-} sub-lattices and rotational modes of PO_4^{3-} group [41]. It has been reported that the appearance of additional bands at 940 and 970 cm^{-1} indicates the presence of β-TCP and α-TCP phases in the structure [42] and a doublet at 941 and 947 cm^{-1} confirms the presence of tetracalcium phosphate (TTCP) phase [43]. Appearance of a doublet at 963 cm^{-1} indicates the existence of HA as well as β-TCP in the material [43]. In the current study, these features

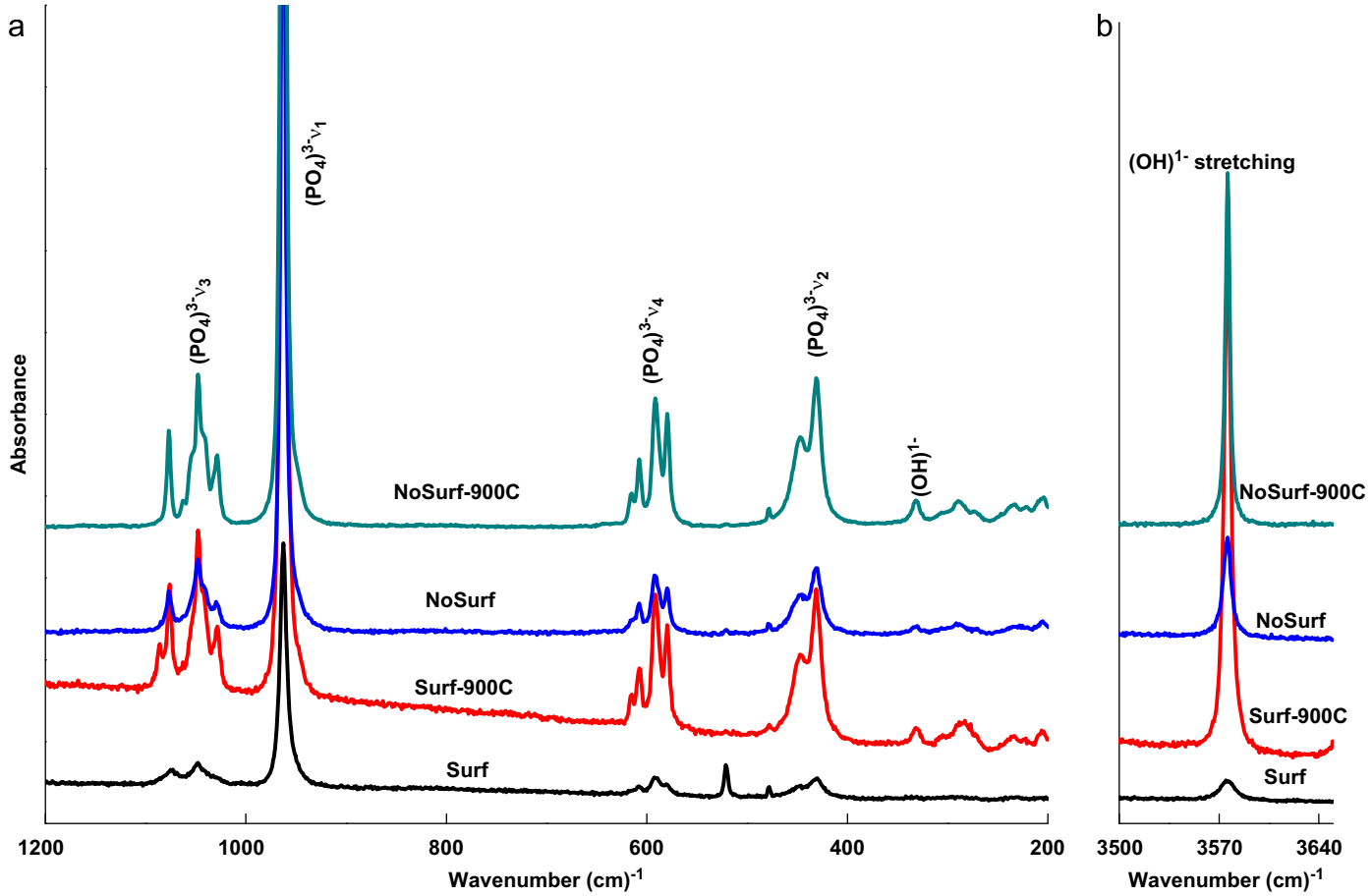

Fig. 8. Raman spectra of synthesized powders: (a) in the scan range 1200–200 cm^{-1} and (b) 3500–3640 cm^{-1}. From bottom to top: powder 'Surf', 'Surf-900C', 'NoSurf' and 'NoSurf-900C'.

are not observed in the Raman spectra of any powder before and after the heat treatment. Therefore, it can be inferred that powders produced by two methods are predominantly in the HA phase. However, one minor β-TCP peak, observed in XRD reflections for powders 'NoSurf' and 'NoSurf-900C' (Fig. 6), is not revealed in Raman spectra. This may be attributed to the lower concentration of β-TCP in these powders.

To appraise the presence of OH^- ions in the synthesized powders, spectra were also collected in the range 3500–3640 cm^{-1} (Fig. 8b). In all the powders a characteristic HA peak was observed at 3576 cm^{-1} which could be attributed to the stretching mode of OH^- group. Whereas, the peak appearing at 335 cm^{-1} (Fig. 8a) is due to translational mode associated with OH^- sub-lattice [41]. The Raman peak appearing at 3576 cm^{-1} is especially sensitive to the crystalline state of HA [44,45]. It is observed that the intensity of this peak increases when the powders are heat treated ('Surf-900C', 'NoSurf-900C'). Moreover, the intensity of this peak is also higher for powder 'NoSurf' as compared to powder 'Surf'. This enhancement in the peak (3576 cm^{-1}) intensity by heat treating and by synthesizing HA powder without surfactant is consistent with XRD results discussed in Section 3.4. It implies that the intensity of the OH^- group peak (at 3576 cm^{-1}) increases with increase in crystallinity and may be used to monitor the crystallinity of HA crystals.

3.6. FTIR analysis

The functional groups associated with HA were also analyzed by Fourier transform infrared spectroscopy (FTIR) and the results are shown in Fig. 9. The IR spectra of calcium apatites mainly consist of phosphate (PO_4), hydroxyl (OH^-) and carbonate (CO_3^{2-}) groups (for carbonated HA) [46,47].

In the FTIR data, the bands appearing at 1097 and 1044, 963, 603 and 564 and 474 cm^{-1} are assigned to the ν_3 (P–O) asymmetric stretching mode, ν_1 (P–O) symmetric stretching mode, ν_4 (O–P–O) bending mode and ν_2 (O–P–O) bending mode, respectively. These assignments are in complete agreement with earlier reports [42,48,49].

Broad bands appearing at around 3450 and 1636 cm^{-1} could be linked to adsorbed or bound water [5]. A sharp peak at 3571 cm^{-1} is associated with OH^- stretching mode and a peak appearing at 632 cm^{-1} is also related with OH^- bending mode [46,48]. The appearance of these two bands in the IR spectra confirms that the powders produced are

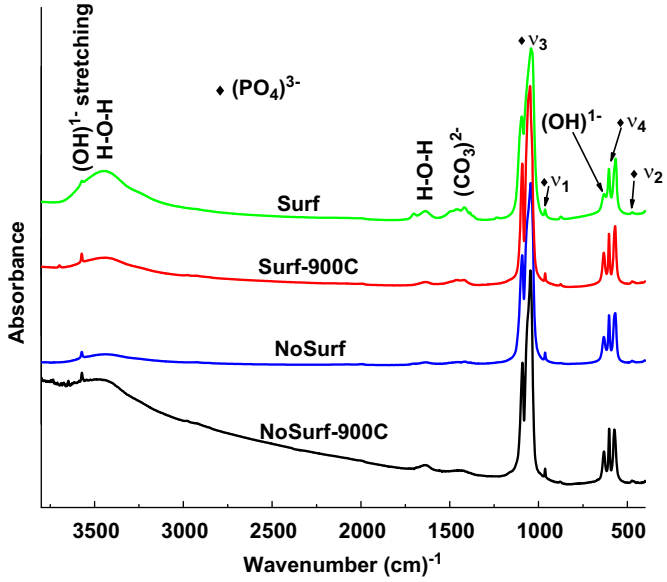

Fig. 9. FTIR spectra of synthesized powders. From bottom to top: Powder 'NoSurf-900C', 'NoSurf', 'Surf-900C' and 'Surf'.

predominantly HA. The intensity of these two bands (3571 and 632 cm^{-1}) is the lowest for the powder synthesized using surfactant ('Surf'; Fig. 9). This decreased intensity of the above mentioned bands may be attributed to the smaller crystallite size for this powder (Fig. 7) and to the incorporation of CO_3^{2-} ions in HA structure [47]. The bands appearing at 1412 and 1456 cm^{-1} are attributed to the presence of CO_3^{2-} ions in the structure [47]. The intensity of CO_3^{2-} ion bands is the highest for the powder produced using surfactant ('Surf'; Fig. 9). This could be linked to the fact that this powder adsorbed more CO_3^{2-} ions from the atmosphere during its synthesis due to its large surface area (Fig. 5a). The decrease in intensity of these CO_3^{2-} ion peaks, with corresponding increase in OH^- ion peaks (3571 and 632 cm^{-1}), is observed when the powders are heat treated. The increase in OH^- intensity by heat treatment has also been observed in Raman spectra (Fig. 8).

Comparing the PO_4^{3-} group peaks appearing in Raman and FTIR analysis, it is noted that all the vibrational modes (v_1, v_2, v_3 and v_4) are resolved by Raman spectroscopy. In FTIR analysis, the v_3 and v_4 modes are prominent, whereas, the v_1 and v_2 modes generate very weak signals as they are IR inactive [50].

Combined Raman and FTIR analyses imply that all the powders are predominantly in the HA phase, crystallinity of the powders increased after heat treatment and powder 'Surf' adsorbed more CO_3^{2-} ions as compared to other synthesized powders.

4. Conclusions

Following conclusions could be drawn:

1. The use of surfactant played an important role; to produce pure HA powders (without β-TCP) and to change the morphology of particles from spherical to needle/rod-like. It also increased the surface area up to three times; consequently more CO_3^{2-} ions were adsorbed on its surface as compared to the powder produced without surfactant.
2. The employment of 60 mM CTAB surfactant produced 10–25 nm diameter and 75–100 nm long HA crystals which are close to HA like crystals found in natural calcified tissues.
3. Heat treatment to 900 °C reduced the surface area and increased the average crystallite size as well as crystallinity degree of HA powders, considerably. A direct correspondence was found between the average crystallite size and the crystallinity degree, though these parameters were measured by two different methods. Moreover, SEM and N_2 adsorption analysis indicated that the powder prepared with surfactant may be more bioactive and better suited for heavy ions removal before the heat treatment.
4. The intensity of OH^- group peak in Raman spectra is highly sensitive to the crystalline state of HA crystals and may be used to gage the crystallinity of the synthesized powder.

References

[1] S.M. Best, A.E. Porter, E.S. Thian, J. Huang, Bioceramics: Past, present and for the future, Journal of the European Ceramic Society 28 (7) (2008) 1319–1327.
[2] M.N. Rahaman, A.H. Yao, B.S. Bal, J.P. Garino, M.D. Ries, Ceramics for prosthetic hip and knee joint replacement, Journal of the American Ceramic Society 90 (7) (2007) 1965–1988.
[3] T.G. Kim, B. Park, Synthesis and growth mechanisms of one-dimensional strontiumhydroxyapatite nanostructures, Inorganic Chemistry 44 (26) (2005) 9895–9901.
[4] Q.J. He, Z.L. Huang, Controlled growth and kinetics of porous hydroxyapatite spheres by a template-directed method, Journal of Crystal Growth 300 (2) (2007) 460–466.
[5] Y.J. Wang, J.D. Chen, K. Wei, S.H. Zhang, X.D. Wang, Surfactant-assisted synthesis of hydroxyapatite particles, Materials Letters 60 (27) (2006) 3227–3231.
[6] P.P. Wang, C.H. Li, H.Y. Gong, X.R. Jiang, H.Q. Wang, K.X. Li, Effects of synthesis conditions on the morphology of hydroxyapatite nanoparticles produced by wet chemical process, Powder Technology 203 (2) (2010) 315–321.
[7] W.C. Xue, S.Y. Tao, X.Y. Liu, X.B. Zheng, C.X. Ding, In vivo evaluation of plasma sprayed hydroxyapatite coatings having different crystallinity, Biomaterials 25 (3) (2004) 415–421.
[8] C. Stotzel, F.A. Muller, F. Reinert, F. Niederdraenk, J.E. Barralet, U. Gbureck, Ion adsorption behaviour of hydroxyapatite with different crystallinities, Colloids and Surfaces B—Biointerfaces 74 (1) (2009) 91–95.
[9] X.D. Zhu, H.J. Zhang, H.S. Fan, W. Li, X.D. Zhang, Effect of phase composition and microstructure of calcium phosphate ceramic particles on protein adsorption, Acta Biomaterialia 6 (4) (2010) 1536–1541.
[10] S.V. Dorozhkin, Bioceramics of calcium orthophosphates, Biomaterials 31 (7) (2010) 1465–1485.
[11] G. Bezzi, G. Celotti, E. Landi, T. La Torretta, I. Sopyan, A. Tampieri, A novel sol–gel technique for hydroxyapatite preparation, Materials Chemistry and Physics 78 (3) (2003) 816–824.

[12] W. Weng, G. Han, P. Du, G. Shen, The effect of citric acid addition on the formation of sol–gel derived hydroxyapatite, Materials Chemistry and Physics 74 (1) (2002) 92–97.
[13] R.R. Rao, H.N. Roopa, T.S. Kannan, Solid state synthesis and thermal stability of HAP and HAP–beta-TCP composite ceramic powders, Journal of Materials Science: Materials in Medicine 8 (8) (1997) 511–518.
[14] S. Pramanik, A.K. Agarwal, K.N. Rai, A. Garg, Development of high strength hydroxyapatite by solid-state-sintering process, Ceramics International 33 (3) (2007) 419–426.
[15] K. Ioku, S. Yamauchi, H. Fujimori, S. Goto, M. Yoshimura, Hydrothermal preparation of fibrous apatite and apatite sheet, Solid State Ionics 151 (1–4) (2002) 147–150.
[16] J.B. Liu, X.Y. Ye, H. Wang, M.K. Zhu, B. Wang, H. Yan, The influence of pH and temperature on the morphology of hydroxyapatite synthesized by hydrothermal method, Ceramics International 29 (6) (2003) 629–633.
[17] Y.J. Wang, S.H. Zhang, K. Wei, N.R. Zhao, J.D. Chen, X.D. Wang, Hydrothermal synthesis of hydroxyapatite nanopowders using cationic surfactant as a template, Materials Letters 60 (12) (2006) 1484–1487.
[18] B. Prélot, T. Zemb, Calcium phosphate precipitation in catanionic templates, Materials Science and Engineering C 25 (5) (2005) 553–559.
[19] G.K. Lim, J. Wang, S.C. Ng, C.H. Chew, L.M. Gan, Processing of hydroxyapatite via microemulsion and emulsion routes, Biomaterials 18 (21) (1997) 1433–1439.
[20] Y.X. Sun, G.S. Guo, D.L. Tao, Z.H. Wang, Reverse microemulsion-directed synthesis of hydroxyapatite nanoparticles under hydrothermal conditions, Journal of Physics and Chemistry of Solids 68 (3) (2007) 373–377.
[21] S.V. Dorozhkin, M. Epple, Biological and medical significance of calcium phosphates, Angewandte Chemie International Edition 41 (17) (2002) 3130–3146.
[22] H. Zhang, M. Zhang, Phase and thermal stability of hydroxyapatite whiskers precipitated using amine additives, Ceramics International 37 (1) (2011) 279–286.
[23] Y. Li, W. Tjandra, K.C. Tam, Synthesis and characterization of nanoporous hydroxyapatite using cationic surfactants as templates, Materials Research Bulletin 43 (8) (2008) 2318–2326.
[24] S. Amin, M. Mujahid, Synthesis of nano hydroxyapatite by chemical precipitation using different surfactant templates, Biomaterials Science—Processing, Properties, and Applications (2011) 67–74.
[25] Y. Pan, D. Xiong, Influence of dispersant and heat treatment on the morphology of nanocrystalline hydroxyapatite, Journal of Materials Engineering and Performance 19 (7) (2010) 1037–1042.
[26] S. Sarfraz, B. Naseem, S. Amin, M. Mujahid, Synthesis and characterization of nano hydroxyapatite, Advanced Materials Research 264 (2011) 1370–1375.
[27] S.X. Ng, J. Guo, J. Ma, S.C.J. Loo, Synthesis of high surface area mesostructured calcium phosphate particles, Acta Biomaterialia 6 (9) (2010) 3772–3781.
[28] C. Qiu, X. Xiao, R. Liu, Biomimetic synthesis of spherical nano-hydroxyapatite in the presence of polyethylene glycol, Ceramics International 34 (7) (2008) 1747–1751.
[29] M. Salarian, M. Solati-Hashjin, S.S. Shafiei, R. Salarian, Z.A. Nemati, Template-directed hydrothermal synthesis of dandelion-like hydroxyapatite in the presence of cetyltrimethylammonium bromide and polyethylene glycol, Ceramics International 35 (7) (2009) 2563–2569.
[30] J. Yao, W. Tjandra, Y.Z. Chen, K.C. Tam, J. Ma, B. Soh, Hydroxyapatite nanostructure material derived using cationic surfactant as a template, Journal of Materials Chemistry 13 (12) (2003) 3053–3057.
[31] M. Törnblom, U. Henriksson, Effect of solubilization of aliphatic hydrocarbons on size and shape of rodlike C16TABr micelles studied by 2H NMR relaxation, The Journal of Physical Chemistry B 101 (31) (1997) 6028–6035.
[32] B. Viswanath, N. Ravishankar, Controlled synthesis of plate-shaped hydroxyapatite and implications for the morphology of the apatite phase in bone, Biomaterials 29 (36) (2008) 4855–4863.
[33] B. Li, B. Guo, H.S. Fan, X.D. Zhang, Preparation of nano-hydroxyapatite particles with different morphology and their response to highly malignant melanoma cells in vitro, Applied Surface Science 255 (2) (2008) 357–360.
[34] A.J. Melville, L.M. Rodríguez-Lorenzo, J.S. Forsythe, Effects of calcination temperature on the drug delivery behaviour of Ibuprofen from hydroxyapatite powders, Journal of Materials Science: Materials in Medicine 19 (3) (2008) 1187–1195.
[35] S. Kannan, A. Lemos, J. Ferreira, Synthesis and mechanical performance of biological-like hydroxyapatites, Chemistry of Materials 18 (8) (2006) 2181–2186.
[36] E. Landi, A. Tampieri, G. Celotti, S. Sprio, Densification behaviour and mechanisms of synthetic hydroxyapatites, Journal of the European Ceramic Society 20 (14–15) (2000) 2377–2387.
[37] Elements of X-ray crystallography, in: L.A. Azaro (Ed.), McGraw-Hill, New York, 1968.
[38] J.B. Park, Bioceramics: Properties, Characterizations, and Applications, Springer Verlag, 2008.
[39] K. Nakamoto, Infrared and Raman Spectra of Inorganic and Coordination Compounds, Wiley Online Library,1978.
[40] R. Cuscó, F. Guitián, S.d. Aza, L. Artús, Differentiation between hydroxyapatite and β-tricalcium phosphate by means of μ-Raman spectroscopy, Journal of the European Ceramic Society 18 (9) (1998) 1301–1305.
[41] Z. Iqbal, V. Tomaselli, O. Fahrenfeld, K. Moller, F. Ruszala, E. Kostiner, Polarized Raman scattering and low frequency infrared study of hydroxyapatite, Journal of Physics and Chemistry of Solids 38 (8) (1977) 923–927.
[42] B. Leon, B. León, J. Jansen, Thin Calcium Phosphate Coatings for Medical Implants, Springer Verlag, 2008.
[43] G.L. Darimont, B. Gilbert, R. Cloots, Non-destructive evaluation of crystallinity and chemical composition by Raman spectroscopy in hydroxyapatite-coated implants, Materials Letters 58 (1-2) (2004) 71–73.
[44] P. De Aza, F. Guitian, C. Santos, S. De Aza, R. Cusco, L. Artus, Vibrational properties of calcium phosphate compounds, 2 Comparison between hydroxyapatite and β-tricalcium phosphate, Chemistry of Materials 9 (4) (1997) 916–922.
[45] L.J. Wang, G.H. Nancollas, Calcium orthophosphates: crystallization and dissolution, Chemical reviews 108 (11) (2008) 4628–4669.
[46] B. Fowler, Infrared studies of apatites. I. Vibrational assignments for calcium, strontium, and barium hydroxyapatites utilizing isotopic substitution, Inorganic Chemistry 13 (1) (1974) 194–207.
[47] M.E. Fleet, X. Liu, Coupled substitution of type A and B carbonate in sodium-bearing apatite, Biomaterials 28 (6) (2007) 916–926.
[48] A. Slosarczyk, C. Paluszkiewicz, M. Gawlicki, Z. Paszkiewicz, The FTIR spectroscopy and QXRD studies of calcium phosphate based materials produced from the powder precursors with different Ca/P ratios, Ceramics International 23 (4) (1997) 297–304.
[49] J.C. Elliot, Structure and chemistry of the apatites and other calcium orthophosphates, Studies in Inorganic Chemistry, vol. 18, Elsevier, 1994.
[50] A. Antonakos, E. Liarokapis, T. Leventouri, Micro-Raman and FTIR studies of synthetic and natural apatites, Biomaterials 28 (19) (2007) 3043–3054.